Engineering Thermoswitchable Lithographic Hybrid Gold Nanorods as Plasmonic Devices for Sensing and Active Plasmonics Applications

Mai Nguyen,[†] Xiaonan Sun,[†] Emmanuelle Lacaze,[‡] Pamina Martina Winkler,[§] Andreas Hohenau,[§] Joachim R. Krenn,[§] Céline Bourdillon,[‡] Azzdine Lamouri,[†] Johan Grand,[†] Georges Lévi,[†] Leïla Boubekeur-Lecaque,[†] Claire Mangeney,*[,†] and Nordin Félidj*[,†]

[†]Laboratoire Interfaces, Traitements, Organisation et Dynamique des Systèmes, Université Paris Diderot, Sorbonne Paris Cité, CNRS UMR 7086, 15 Rue Jean-Antoine de Baïf, 75205 Paris Cedex 13, France

[‡]Laboratoire INSP, Université Pierre et Marie Curie, 5 Place Jussieu, 75005 Paris, France

[§]Institut für Physik, Karl-Franzens-Universität Graz, Universitätsplatz 5, 8010 Graz, Austria

S *Supporting Information*

ABSTRACT: In this article, we aim to investigate the sensitivity of regular arrays of hybrid plasmonic nanostructures to variations in properties of the local environment (temperature, refractive index, polymer thickness), in the context of sensing and active plasmonic applications. A proper description and characterization of such hybrid systems is indeed essential in order to provide designed criteria for efficient stimuli-responsive devices. As an ideal model, we introduce a novel kind of hybrid plasmonic core–shell system made of lithographic gold nanorods (GNRs), coated by a thermosensitive polymer shell based on poly(N-isopropylacry-

lamide) (pNIPAM). The grafting of the polymer on the GNRs results from a multistep but simple approach in order to confine the pNIPAM brushes on the GNRs and to control the thickness of the polymer coating. We show that the optical response of the plasmonic hybrid structures (GNR@pNIPAM) is strongly modified upon a variation of the external temperature, due to a physical change of the conformation of the polymer coating. These thermo-induced changes of the optical properties can be optimized by changing the aspect ratio of the GNRs and the polymer thickness to obtain very efficient optical reporters of the polymer state in a controlled and reversible manner. This work could provide an important step toward the use of GNR@pNIPAM structures for applications spanning from opto-mechanical modulators to nanoscale adhesion and molecular sensing.

KEYWORDS: *lithographic gold nanorods, thermosensitive polymer, plasmonic properties, discrete dipole approximation*
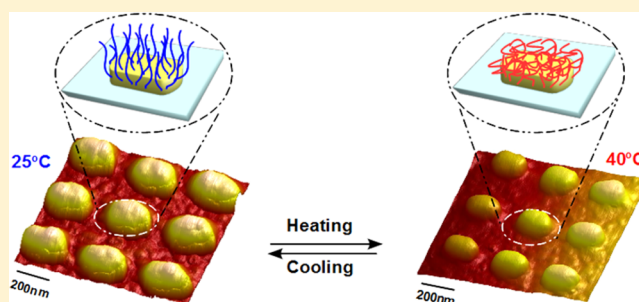
The patterning of inorganic nanomaterials combined with soft matter can give access to a fascinating class of hybrid structures and properties, in which the stimuli-responsive properties of the soft component can drastically modify the electrical, magnetic, optical, or catalytic properties of the inorganic component.[1,2] If the hybrid system is made of gold or silver nanostructures coated with polymeric shells, their optical properties can be dynamically modified or switched provided that an external stimulus (pH, temperature, electrical conductivity, light, etc.) impacts the physical or chemical properties of the polymer.[3−7] These optical properties are governed by the excitation of localized surface plasmon (LSP) modes, corresponding to a collective oscillation of the conduction electrons at the particle surface.[8] As a result, a large extinction cross-section emerges at the resonance, in the visible or near-infrared region (mainly for gold, silver, and copper).[9] The frequency of the LSP mode strongly depends on the size and the shape of the metallic particles, the interparticle distance, and the refractive index of the surrounding medium.[10] In particular, the sensitivity of the plasmonic structures to a

tunable surrounding medium is the main criterion for the development of *active* plasmonic applications.[11,12] These "smart" nanomaterials have recently shown great potential in many applications such as optical switches at the nanoscale,[13] surface-enhanced spectroscopies (Raman scattering or fluorescence),[14] molecular sensing,[15] and drug delivery.[16]

Because of the different properties of the soft matter and the inorganic part, the hybrid systems present a high degree of complexity.[17] In order to understand and optimize the physical and chemical properties of both inorganic/organic components, a fundamental study of their combined performances is required. This fundamental study is possible provided that we consider the design of perfectly calibrated hybrid systems with a precise control of the particle geometry,[18] as well as a control of the thickness of the polymer shell. The combination of lithographic arrays of gold nanoparticles sustaining LSP modes with a thermosensitive polymer, poly(N-isopropylacrylamide)

(pNIPAM), represents a good model for such hybrid systems. The thermosensitive polymer exhibits a temperature-dependent solution and surface behavior. It corresponds to a reversible and abrupt phase transition upon going from a swollen conformational state to a collapsed state around its lower critical solution temperature (LCST) at 32 °C in pure water.[19,20] The time scale for this transition has been estimated to be ~1 ms.[21,22] This temperature-induced polymer phase transition is associated with a hydrophilic to hydrophobic switch. Therefore, conformational changes of pNIPAM brushes, when varying the external temperature, are expected to achieve dynamic and reversible tuning of the LSP resonance frequency, due to a change in the local refractive index around the particles.[23−26]

Up to now, most of the proposed hybrid systems with pNIPAM were made of colloidal systems in aqueous solution or assembled in two-dimensional disorganized substrates,[24] which represent a central obstacle for fundamental investigations and extensive applications. More recently, ordered arrays of silver particles covered by pNIPAM were proposed to facilitate the investigation of the nanoparticle coupling.[27] However, to our knowledge, no extensive experimental studies have been made on the influence of the particle geometry and the polymer thickness on the optical performances of the hybrid systems. The effect of the polymer shell thickness on the LSP wavelength shift was studied only theoretically by M. Tagliazucchi et al., evidencing a clear correlation between both parameters.[28]

Many efforts have been invested in order to identify plasmonic structures with a larger spectral LSP shift upon a change of the local environment. Among them, gold nanorods (GNRs) remain very favorable for plasmonic applications. Indeed, the LSP wavelength can be finely tuned by changing the GNRs aspect ratio and presents a strong extinction efficiency due to a low LSP damping.[29] In this work, we aim to develop a novel kind of hybrid core−shell plasmonic nanoparticles (NPs) with the following desired characteristics: (i) a strong sensitivity to the local refractive index through the design of regular arrays of GNRs, (ii) an organic shell confined on the GNRs and presenting a high density of polymer chains to allow for the phase transition between the swollen and collapsed regime,[17] and (iii) a controlled thickness of the polymer layer, which can be adjusted by the polymerization time.[30] Another important aspect that should be considered here for obtaining robust hybrid structures stable over time is the chemical nature of the link between the pNIPAM brushes and the GNR surface. A strong covalent coupling between the stimulable organic coating and the GNRs should be promoted, in order to investigate in a fully reversible manner the influence of the organic shell on the tuning of the LSP resonance wavelength, when varying the temperature.[31,32] We address these issues by considering regular arrays of gold nanorods of different aspect ratios designed by electron-beam lithography (EBL), deposited on an indium−tin oxide (ITO)-covered glass substrate.[33] The GNRs were covered by a polymer shell through a well-established strategy, developed in our group, based on initiators derived from diazonium salts and a polymerization method called surface-initiated atomic transfer radical polymerization (SI-ATRP).[34] This chemical strategy enables the confinement of the pNIPAM brushes exclusively on the GNRs and not on the underlying ITO substrate. Atomic force microscopy (AFM) images recorded in air and in water at different temperatures allowed us to investigate the core−shell characteristics of the GNR@pNIPAM structures as well as their

dynamic behavior by changing the external temperature. The optical properties of the GNR@pNIPAM samples versus the external temperature were investigated on GNRs of different aspect ratios and different polymer shell thicknesses. This study highlights the importance of a proper description of these parameters in order to provide optimized GNR@pNIPAM structures for the design of efficient chemical sensors with architectural control.[35]

■ RESULTS AND DISCUSSION

Elaboration and Description of the GNR@pNIPAM Core−Shell Systems. The GNR arrays were produced by EBL. A 90 nm thick layer of PMMA (poly(methyl methalcrylate)) was spin-casted onto a transparent ITO-coated glass substrate.[33] After chemical development of the exposed areas, thermal evaporation of gold and a lift-off procedure followed. The EBL technique enabled us to control the GNR arrangement on the substrate (interparticle distance Λ = 280−300 nm), as well as their aspect ratio, defined as $r = a/b$ (a and b represent the particle in-plane long and short axes, respectively). In our study, the aspect ratio varies from 1.1 to 2.8, and the NP height (~50 nm) is kept constant over the different arrays. Typical scanning electron microscope (SEM) images of the obtained arrays are depicted in the Figure 1a, with a description of their optical response (Figure 1b) and geometrical features (Table SI.1). Their optical response was probed by far-field extinction microspectroscopy in the 500−900 nm range. The spectrometer is coupled to an upright optical microscope equipped with a 50× objective (numerical aperture (NA) = 0.35). The investigated area was approximately 80 μm in diameter, which is smaller than the array dimensions (100×100 μm^2). Due to their anisotropic shape, the optical response of the bare GNRs is characterized by two LSP modes: a transverse LSP mode located at 530 nm (in air) for an incident polarization along the short axis b and a longitudinal LSP mode for an incident polarization along the main axis a. The latter mode is very sensitive in wavelength to the local environment and to the aspect ratio, varying from 540 to 800 nm when increasing r from 1.1 to 2.8 (see Figure 1b). We have thus mainly focused our attention on the longitudinal LSP mode in our optical studies.

Our strategy for the surface modification of GNR arrays is depicted in the Supporting Information (Figure SI.1a). It involves the following steps: (i) A spontaneous covalent grafting of hydroxyl (−OH)-terminated aryl moieties occurs on the surface of the GNRs. This is achieved on a cleaned GNR-coated ITO substrate by incubation with 4-hydroxyethylbenzene diazonium tetrafluoroborate salt in water at room temperature. (ii) The terminal hydroxyl groups are treated with 2-bromoisobutyryl bromide (0.1 M, toluene) in the presence of triethylamine (0.12 M) for 5 min, leading to bromo-terminated ester groups able to initiate the polymerization of NIPAM. Using this approach, the grafting of the SI-ATRP initiators could be confined exclusively on the gold nanoparticle surface. The spontaneous grafting of the aryl layers derived from diazonium salts was found to be inefficient on the underlying ITO substrate, which remained uncovered during the whole functionalization procedure, as demonstrated by XPS spectroscopy (see Figure SI.2). (iii) pNIPAM brushes are grown from the initiator-covered GNRs using standard aqueous SI-ATRP conditions.[34] This procedure, detailed in the Experimental Section, allows the control of the pNIPAM thickness, by exposing the initiator-modified surface to a

(a)

(b)
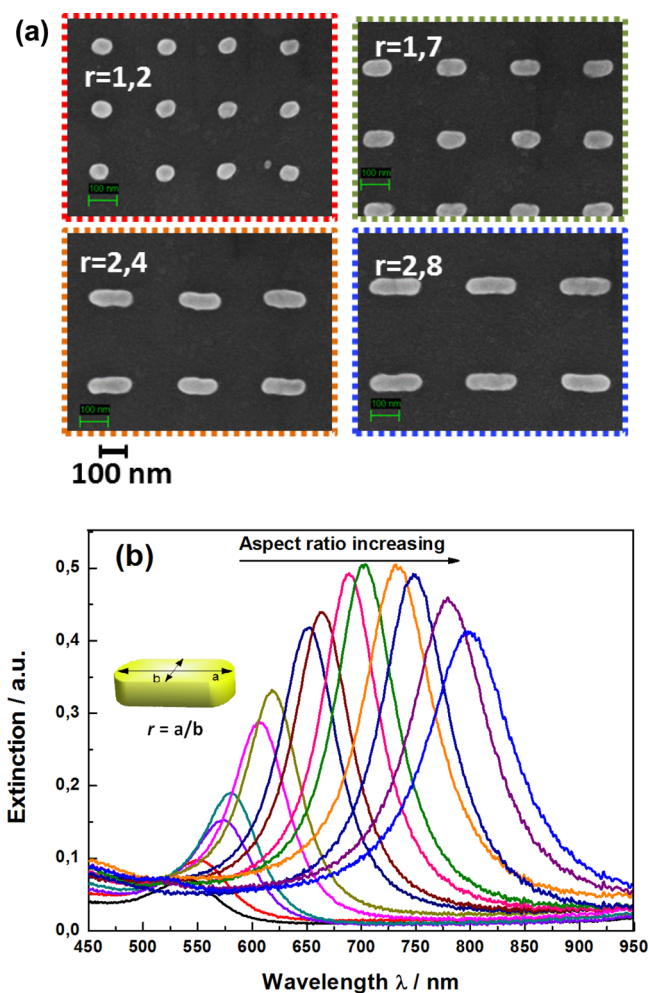
Figure 1. (a) SEM images of a few examples of lithographic arrays of gold bare nanorods (GNRs) investigated in this work, with increasing aspect ratios r (from left to right). (b) Extinction spectra of the GNRs with aspect ratios increasing (from left to right). The spectra are recorded with an incident polarization parallel to the main axis, in air. The longitudinal LSP mode is red-shifted from 540 to 800 nm, when r goes from 1.1 to 2.8.

polymerizing solution of *N*-isopropylacrylamide for various times (at room temperature). Finally, it ensures homogeneous polymer layers with high grafting density. Indeed, in a previous work, we showed that the surface coverage of initiators was estimated to be 10 molecules/nm^2 by XPS spectroscopy, which is high enough for the growth of dense polymer layers.[30]

Choice of the pNIPAM Shell Thickness. As previously observed in the literature, the optical response of core−shell plasmonic systems is expected to depend on the thickness of the dielectric shell.[36] In order to understand, for a given GNR core, the influence of the shell thickness on the LSP wavelength, extinction data have been correlated with the discrete dipole approximation (DDA) simulations.[37,38] This model allows calculating the LSP resonance wavelength of a gold/dielectric target for different dielectric shell thicknesses. The target includes (i) a gold rectangle ended by two hemispherical edges (height = 50 nm, main axis = 112 nm, short axis = 60 nm, aspect ratio r = 1.87). This target has been built since its shape is close to the GNR geometrical features studied in this work. The target also includes (ii) a dielectric overlayer coating of different thicknesses (varying from 0 to 40

nm), with a refractive index of n = 1.4 (close to the refractive index of the thermosensitive polymer in the collapse regime). Finally, the whole target is immersed in water (with a refractive index of n = 1.33). Details on the DDA calculations are indicated in the Experimental Section. At this point, it is important to note that, to simulate the phase transition of pNIPAM for the two states of pNIPAM (on both sides of the LCST), the GNR@pNIPAM structures were modeled by two different systems, as illustrated in Figure 2a: (a) Below the LCST temperature, the pNIPAM brushes are fully swollen by water and their refractive index is close to n = 1.33. Therefore, the GNR@pNIPAM structures are modeled by bare gold targets surrounded by water. (b) Above the LCST, the pNIPAM brushes are collapsed and form an organic shell with a higher refractive index (close to 1.4 as measured in previous works).[17] The hybrid structures are thus modeled by a core−shell target immersed in water (with a shell refractive index of n = 1.4). The DDA calculations show that the LSP wavelength varies from 674 nm (for a bare gold target array) to 696 nm (for a gold target array covered by a 40 nm dielectric shell thickness), as shown in Figure 2b. For dielectric shells thicker than 40 nm, the LSP wavelength red-shift is quasi-saturated (reaching 698 nm for an infinite dielectric thickness). Therefore, a maximum LSP shift (between the bare particle in water and the core−shell particle) of $\Delta\lambda_{\mathrm{LSP}}^{\mathrm{DDA}} \approx 24$ nm is obtained for a shell thickness greater than 40 nm (Figure 2b). The DDA calculations indicate that an optimized polymer thickness around the GNRs should be ∼40 nm in the collapsed regime, in order to obtain a maximum LSP wavelength shift $\Delta\lambda_{\mathrm{LSP}}^{\mathrm{LCST}} = \lambda_{\mathrm{T>LCST}} - \lambda_{\mathrm{T<LCST}}$ ($\lambda_{\mathrm{T>LCST}}$ and $\lambda_{\mathrm{T<LCST}}$ representing the LSP wavelengths above and below the LCST, respectively), between the collapsed and swollen regimes, respectively.

Since the SI-ATRP method allows control of the polymer thickness, we proposed in this work to achieve two sets of GNR arrays of similar aspect ratios (varying from r = 1.1 to 2.8), with two different organic shell thicknesses, in order to analyze the influence of the organic thickness. (i) In a first set of arrays (sample A), the polymer coating was chosen to be relatively thick, with a thickness of ∼50 nm in the collapsed regime, in order to obtain a large LSP shift, in agreement with the DDA calculations. (ii) In contrast, in a second set (sample B), a very thin layer of polymer (∼10 nm, in the collapsed state) has been grafted on identical GNRs. Details of the procedure for grafting the polymer brushes on samples A and B are indicated in the Experimental Section.

AFM Characterization. Before grafting the organic shell on the gold GNR arrays, the height of the GNRs was estimated by AFM microscopy (see Figure SI.3a for GNRs with an aspect ratio of 2.3). A height of 50 nm was deduced from the cross section, and it was observed to vary by less than ±1 nm on the whole sample (Figure SI.3b).[39] To verify that the pNIPAM growth could be confined exclusively around the GNRs and not on the underlying ITO substrate, gold model and ITO substrates were submitted to the pNIPAM grafting protocol and then characterized by X-ray photoelectron spectroscopy (XPS). The XPS spectra revealed that the bromo-terminated groups were present on gold, while ITO appeared to be free from bromide, confirming the confinement of the organic coating around the GNRs (Figure SI.2). In order to measure the polymer thickness, the AFM images of the functionalized GNR array have been recorded in air for samples A and B. We have first measured the initiator thickness for both samples. We found 25 ± 1.5 nm for sample B and 3 ± 1 nm for sample A
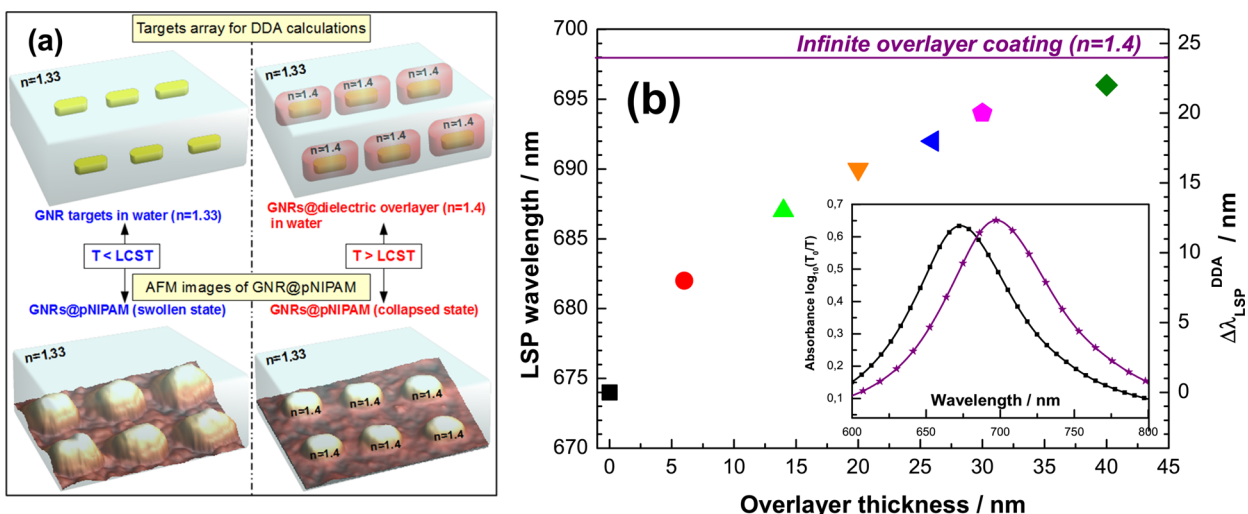
Figure 2. (a) Scheme of the target array modeled for the DDA calculations: (i) Below the LCST, the GNR@pNIPAM structures are represented by bare gold targets in a medium of refractive index $n = 1.33$; (ii) above the LCST, the hybrid structures are represented by a core−shell target in water, wih a shell of refractive index $n = 1.4$. (b) Calculated longitudinal LSP red-shift for the gold targets (main axis: 112 nm, short axis: 60 nm, height: 50 nm), coated by the dielectric overlayer (OVL) of different thicknesses H_{OVL} (OVL of refractive index $n = 1.4$): from $\lambda_{LSP}^{DDA} = 674$ nm for $H_{OVL} = 0$ nm to $\lambda_{LSP}^{DDA} = 698$ nm for an infinite dielectric thickness; the LSP shift $\Delta\lambda_{LSP}^{DDA}$ between the gold target coated by the OVL and the bare gold target is also represented. The maximum of $\Delta\lambda_{LSP}^{DDA}$ (~24 nm) is obtained for an infinite dielectric OVL. Inset: Two examples of calculated absorbance spectra of a gold target: (black graph) immersed in water; (purple graph) covered with a dielectric OVL ($n = 1.4$) of 40 nm (the target is immersed in water).

(Table 1). Therefore, the AFM images allow one to estimate the shell height (including the initiator and the pNIPAM), with

Table 1. Height of the GNRs (Aspect Ratio $r = 2.3$) at the Different Polymerization Steps, Including the pNIPAM Coating for Samples A and B[a]

sample	bare GNRs	GNRs with initiator (initiator thickness)	GNRs with dried pNIPAM (thickness h_{dry})	GNRs with swollen pNIPAM (nm) (thickness $h_{swollen}$)
sample A	50 ± 1 nm	75 ± 1.5 nm (25 nm)	100 ± 2 nm (25 nm)	125 ± 2 nm (50 nm)
sample B	50 ± 1 nm	53 ± 1 nm (3 nm)	61 ± 1 nm (8 nm)	76 ± 2 nm (16 nm)

[a]The measurements have been deduced from the cross section profile of the AFM images (Figure 3e).

a thickness of 50 ± 2 nm for sample A and 11 ± 1 nm for sample B (Figure 3a and c). Those heights were deduced from the cross section profile of the AFM images (see Figure 3e). Note that the height of the dried organic coating (measured in air) reflects the sum of the thickness of the initiator layer and the polymer brushes. The dried thickness of the PNIPAM brushes is ca. 25 ± 2 nm for sample A and ca. 8 ± 1 nm for sample B. Table 1 summarizes the height of the GNRs at the different polymerization steps, for both samples.

The AFM images recorded in air correspond to a regime where pNIPAM is in a collapse state, because it free from water. It should therefore be comparable to the collapsed regime in water above the LSCT. In order to estimate the polymer thickness in the brush regime (at a temperature below 32 °C), we recorded the AFM images of the same GNR arrays in aqueous solution at ~25 °C (Figure 3b and d). The AFM images reveal a thickness of swollen pNIPAM brushes of 50 nm for sample A (thickness of 75 nm including the initiator) and

16 nm for sample B (thickness of 26 nm including the initiator).

From the swelling ratio, defined as $\alpha = h_{swollen}/h_{dry}$, one could extract the molecular parameters of pNIPAM.[40] Indeed, the Alexander−de Gennes model describes the behavior of polymer brushes in good solvent.[41,42] In this model, the dry thickness h_{dry} is linked to the grafting density by eq 1:

$$h_{dry}d^2 = Na^3 \tag{1}$$

where d is the average distance between the tethered chains ($1/d^2$ is the grafting density), N is the number of monomer units per chain, and a is the monomer size.

In contrast, the swollen brush is pictured as formed of stretched chains subdivided into blobs of size $D_b \sim d$ (see scheme of Figure SI.1b). The blob size is given by eq 2:

$$D_b = g^\nu a \tag{2}$$

where g is the number of monomers in a blob, and ν is the Flory exponent.[20] The swollen brush thickness corresponds to eq 3:

$$h_{swollen} = n_b D_b \tag{3}$$

where $n_b = N/g$ is the number of blobs per chain. Replacing D_b by d in eqs 2 and 3 gives the following equation for the swollen thickness:

$$h_{swollen} = Na(d/a)^{1-1/\nu} \tag{4}$$

The swelling ratio therefore corresponds to eq 5:

$$\alpha = h_{swollen}/h_{dry} = (d/a)^{3-1/\nu} \tag{5}$$

The exponent ν was chosen close to 1/2, considering a dense brush regime. Assuming the monomer size to be $a \approx 5$ Å,[43] one could then estimate the average distance between individual brushes (d), the grafting density ($1/d^2$), the number of monomer units per chain (N), and the average molecular weight of the grafted chains (M_n) (see Table 2).
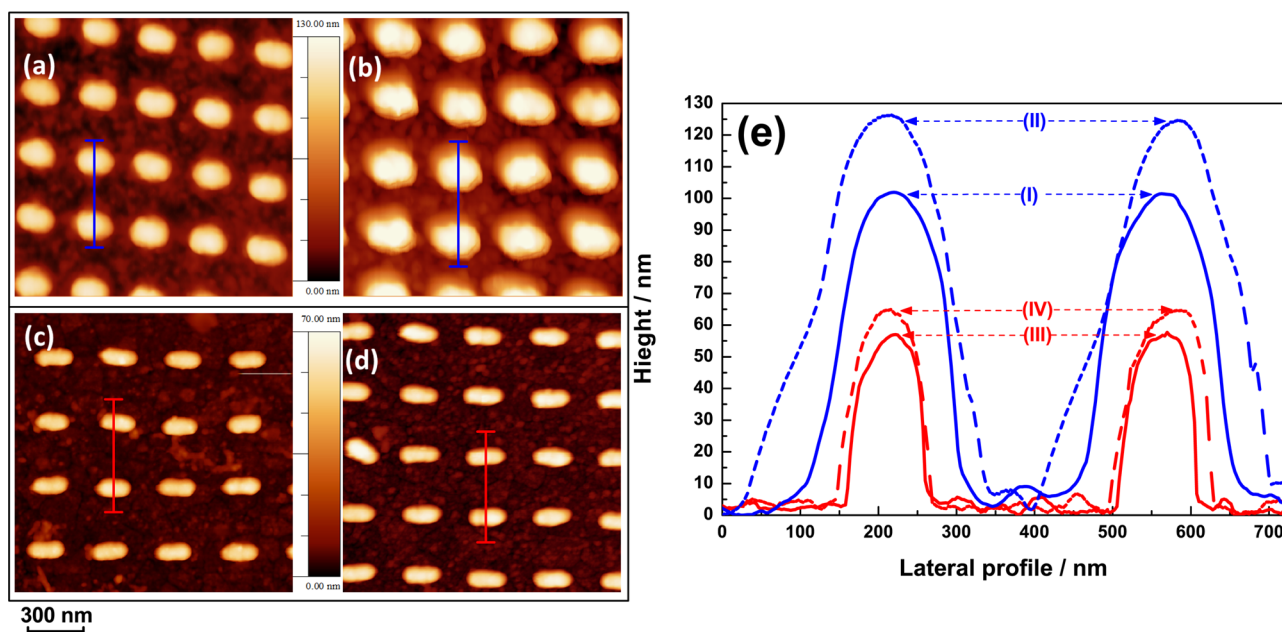
Figure 3. AFM images of a GNRs@pNIPAM lithographic array with an aspect ratio = 2.3, recorded at room temperature: (a) sample A in air (collapsed state of the polymer); (b) sample A in water (swollen state of the polymer); (c) sample B in air (collapsed state of the polymer); (d) sample B in water (swollen state of the polymer). (e) Profile of the cross sections of the samples, including two GNRs, from the AFM images: (I) sample A in air (blue solid line) and (II) in water (blue dashed line). The height of the pNIPAM has been estimated as ∼25 nm in air (I) and ∼50 nm in water (II). Sample B: (III) in air (red solid line), (IV) in water (red dashed line). The height of the pNIPAM has been estimated as ∼8 nm in air (III) and ∼16 nm in water (IV).

Table 2. Molecular Parameters of pNIPAM Brushes

| sample	h_{dry} (nm)	swelling ratio α	grafting density (chains nm^{-2})	N	mean molecular weight, M_n
A	25	2	1.4	143	∼16 180
B	8	2	1.1	458	∼6560

While AFM demonstrates the efficient grafting of the pNIPAM brushes on the array of GNRs@pNIPAM and the confinement of this polymer coating exclusively on the gold nanoparticle surface, the molecular parameters estimated from the Alexander−de Gennes model show that the grafting densities are high and that the swelling ratios ($\alpha \approx 2$) are similar for both samples despite a different initiator layer thickness.

UV−Visible Absorption Characterization. To highlight the sensitivity of the GNRs to the local surrounding medium, we compared the UV−visible absorption spectra of GNR arrays of different aspect ratios in air, before and after the polymerization process (see Figure SI.4). One observes a red-shift of the longitudinal LSP wavelength $\Delta\lambda_{LSP}$ after addition of the polymer coating (Figure SI.4a). This red-shift is attributed to an increase of the local refractive index around the GNRs in the presence of the polymeric layer. This shift is even more important for higher aspect ratios (Figure SI.4b). This larger LSP red-shift is strongly related to the higher sensitivity of anisotropic plasmonic structures to the surrounding medium, as previously mentioned in the literature.[44] Interestingly, it seems that the maximum LSP shift takes place for GNR arrays with aspect ratios ranging from 2.4 and 2.6, although not clearly pointed out in Figure SI.4b. Note that similar maximum LSP shifts have been also reported by J. Becker et al. using gold colloidal GNRs of given aspect ratios.[29] The LSP maximum shifts were obtained for aspect ratios ranging from 3 to 4. This difference from our results can be explained by the fact that the

lithographic GNRs are different in shape, in comparaison with the colloidal rod-shaped NPs. These maximum LSP shifts have been interpreted as a higher quality factor of the LSP band, resulting in a more sensitive dependency on changes in the local environment. Finally, for a given aspect ratio r, the LSP red-shift is much less important when the shell thickness is thinner (up to 35 nm for sample B, compared to ∼100 nm for sample A, for a given GNR aspect ratio of $r = 2.6$), which is in good qualitative accordance with the DDA calculations (Figure SI.4c).

Thermoinduced Modifications of the Optical Properties of GNR@PNIPAM upon Bulk Solution Heating. Two important parameters were selected in order to study their influence upon the sensitivity of the optical properties of GNR@pNIPAM to changes in temperature: (i) the GNR aspect ratio and (ii) the pNIPAM brush thickness.

i. Influence of the GNRs Aspect Ratio. The influence of the aspect ratio of GNRs on their optical response was analyzed on sample A, below and above the LCST. A red-shift of the longitudinal LSP wavelength is observed for the whole GNR arrays, when the temperature increases from 18 °C to 52 °C. It is noteworthy that, since temporal temperature gradients are very small and pNIPAM is thin, thermal equilibrium between water and GNRs should be reached within nanoseconds to microseconds.[45] This red-shift is due to an increasing of the refractive index of the surrounding medium above the LCST (32 °C). Indeed, the polymer density, at the vicinity of the particle surface, is higher in the collapsed regime, as already mentioned in previous works.[24] Figure 4a shows an example of the temperature-dependent extinction spectra of a GNR arrays with $r = 1.8$. The LSP shift $\Delta\lambda_{LSP}^{LCST}$, between the collapsed and brush regimes, is ∼14 nm. It is in good qualitative agreement with the DDA calculations considering a gold target such as $r = 1.8$, with a 26 nm dielectric shell thickness immersed in water,
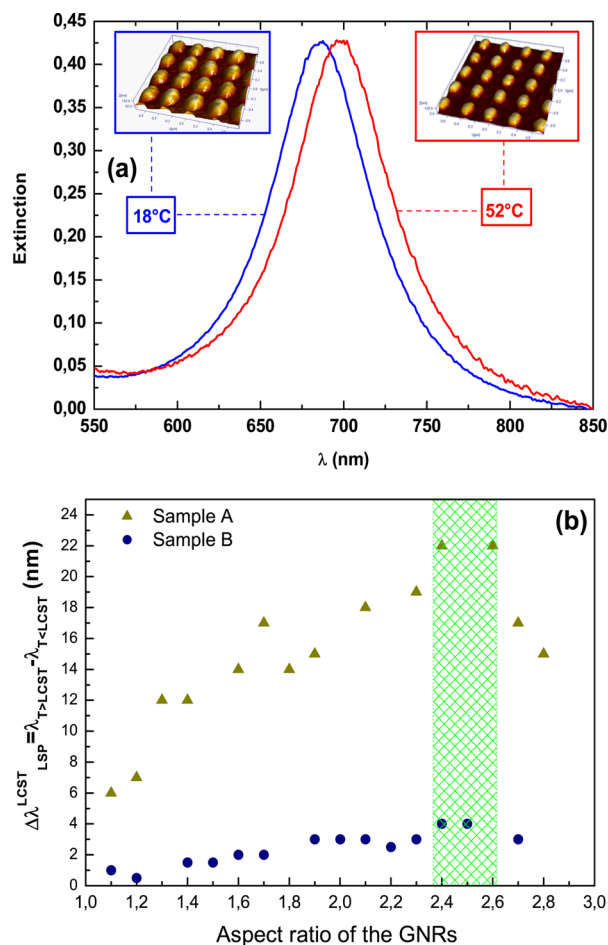
Figure 4. (a) Extinction spectra of a GNRs@pNIPAM array displaying the longitudinal LSP mode (aspect ratio r = 1.8, sample A) at 18 °C (in blue) in the swollen regime, below LCST, and at 52 °C (in red) in the collapsed regime, above LCST. The $\Delta\lambda_{LSP}^{LCST}$ is ~14 nm. (b) Plot of $\Delta\lambda_{LSP}^{LCST}$ versus the aspect ratio of the GNRs for samples A (triangles) and B (circles). The maximum of $\Delta\lambda_{LSP}^{LCST}$ is observed for aspect ratios r between 2.4 and 2.6 for sample A (indicated with the green dashed zone). For sample B, the maximum of LSP shift is less obvious, although pointed out in the dashed zone.

for which an LSP shift $\Delta\lambda_{LSP}^{DDA}$ of ~16 nm was obtained (Figure 2). $\Delta\lambda_{LSP}^{LCST}$ is even more pronounced when increasing the aspect ratio, reaching 22 nm for r = 2.6, due to the higher environmental sensitivity of the GNRs (Figure 4b). Note that the LSP shifts $\Delta\lambda_{LSP}^{LCST}$ are less important in comparison with the LSP shifts $\Delta\lambda_{LSP}$ after polymerization (Figure SI.4b). This is related to a lower change in refractive index Δn of the surrounding medium in the case of $\Delta\lambda_{LSP}^{LCST}$ ($\Delta n \approx 0.06$), to be compared to $\Delta\lambda_{LSP}$ ($\Delta n \approx 0.4$). For aspect ratios higher than r = 2.6, the LSP shift decreases (down to $\Delta\lambda_{LSP}^{LCST} \approx 15$ nm for r = 2.8, sample A), due to a decrease in the quality factor of the LSP resonance.

ii. Influence of the Organic Shell Thickness. Another important factor is the control of the thickness of the polymer shell. For a fixed aspect ratio, we now compare the LSP shift $\Delta\lambda_{LSP}^{LCST}$ between the collapsed and swollen regimes for samples A and B (see Figure 4b). As clearly observed, a decrease in shell thickness leads to a significant decrease in the LSP shift for all the sets of GNRs. As an example, $\Delta\lambda_{LSP}^{LCST}$ decreases from 20 nm to 3 nm for GNRs of identical aspect ratio (r = 2.4; see Figure SI.5). This observation is in good qualitative agreement with

DDA calculations which show that $\Delta\lambda_{LSP}^{DDA}$ between the LSP wavelength of the core−shell gold target and the LSP wavelength of a bare gold target is lower when the shell thickness is smaller.

Optical Reading of the pNIPAM Phase Transition. Due to their high sensitivity to the local environment, the GNR@pNIPAM structures highlight their potential as efficient structures for reporting the thermosensitive polymer state. In order to investigate the phase transition LCST, the extinction spectra were recorded versus the external temperature for both samples A and B. See for instance the extinction spectra of the GNRs (r = 2.4, sample A) in Figure SI.6, for which a progressive LSP red-shift is observed as the temperature increases. The temperature dependence of the LSP red-shift is plotted in Figure 5 for two arrays of GNRs in sample A of
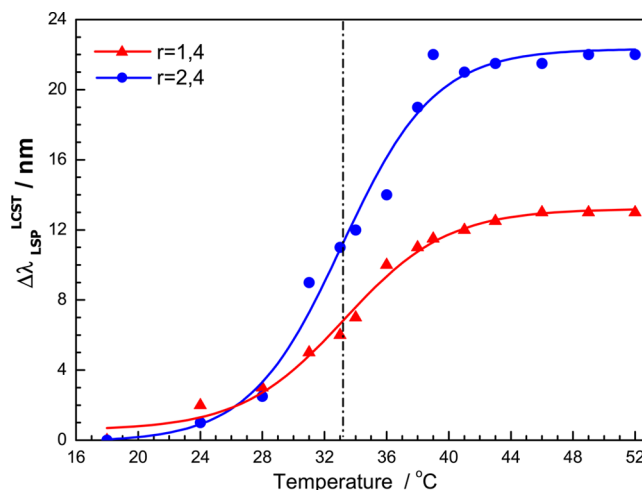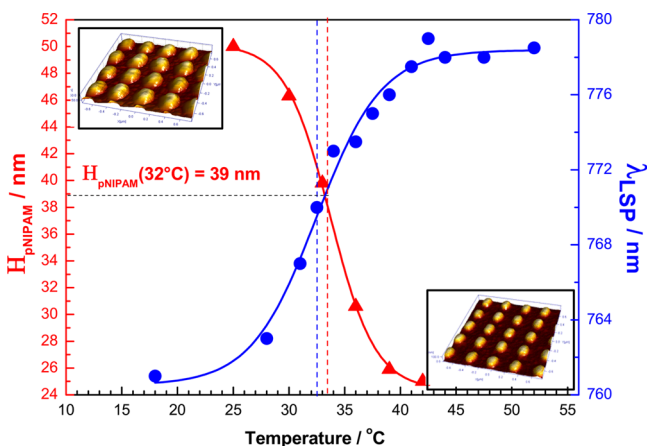

Figure 5. Plot of the temperature dependence of the LSP wavelength $\Delta\lambda_{LSP}^{LCST}$, measured in water, for GNR arrays with two different aspect ratios: r = 1.4 and r = 2.4 (sample A). For GNRs with r = 1.4, the red triangles represent the experimental data, and the red full line, the sigmoid curve fitting the experimental data. For GNRs with r = 2.4, the blue circles represent the experimental data, and the blue full line, the sigmoid curve fitting the experimental data. The maximum values deduced from the derivatives of the sigmoids represented with a vertical dashed line are found at ~33 °C for both GNR arrays r = 1.4 and r = 2.4.

different aspect ratios: r = 1.4 and 2.4. The experimental data can be nicely fitted by a sigmoid curve. The two curves display two plateau regions below and above the phase transition and an abrupt transition in between. One can note that the slope of the sigmoid, in the intermediate region, is much more important for GNRs of aspect ratio r = 2.4 than for GNRs of aspect ratio r = 1.4. This higher slope is due to a stronger sensitivity to the local environment for GNRs of aspect ratio r = 2.4. The graphs of the LSP shift versus the temperature is presented in Figure SI.7a for the whole set of GNR arrays, showing that the slope of the sigmoid is higher as the aspect ratio increases. Note that all the data presented in Figure SI.7a correspond to the longitudinal LSP wavelength versus the temperature. As previously mentioned, if one considers the transversal LSP mode wavelength, its sensitivity to the local environment, and thus to the collapse of the pNIPAM, is much weaker, as displayed in Figure SI.8.

In order to report more properly the maximum of slope of the sigmoids, the derivative of the sigmoid curves versus the

temperature has been calculated (curves not shown). The maxima are indicated with a vertical dashed line in Figure 5. Interestingly, it is found that the maximum is located at ∼33 °C for both arrays, corresponding to the LCST.

In order to estimate the height of the pNIPAM at ∼33 °C, we combined our optical measurements with AFM measurements in water at temperatures varying from 25 to 42 °C (for the GNR array r = 2.3 in sample A). Moreover, the AFM measurements allow us to link the observed spectroscopic shifts to the actual pNIPAM thicknesses. The variation of pNIPAM thickness versus the temperature is reported in Figure 6. As


Figure 6. In red triangles: temperature dependence of the height of the pNIPAM, measured by AFM (the experimental data are fitted by a sigmoid curve, in red solid line). In blue dots: temperature dependence of the longitudinal LSP wavelength (the experimental data are fitted by a sigmoid curve, in blue solid line). The vertical dashed red and blue lines represent the maximum of the derivative of the sigmoid curves from the temperature dependence of the pNIPAM height and the LSP wavelength, respectively.

clearly shown from the AFM measurements, the pNIPAM thickness is decreasing from ∼50 nm in the swollen regime at 25 °C to ∼25 nm in the collapsed regime at 42 °C, with an abrupt slope between 28 and 37 °C. Interestingly, the pNIPAM height, from the AFM data, can also be nicely fitted by a sigmoid, with the derivative (absolute value) displaying a maximum at ∼33 °C (dashed vertical blue line). Remarkably, the maxima of the two slopes (deduced from AFM and spectroscopic measurements) are obtained for the same temperature, ∼33 ± 0.5 °C (see Figure 6). The combination of the AFM and spectroscopic measurements allows us to properly separate the temperature range of the two polymer states. Moreover, the AFM measurements allow us to estimate the thickness of the pNIPAM, h_{pNIPAM}, separating the two regimes. We found $h_{pNIPAM} \approx$ 39 nm at ∼33 °C, which corresponds to 50% of the height of the pNIPAM in the swollen regime. Note that this thermo-induced response was shown to be fully reversible over repeating cycles of temperatures decreases from 52 °C to 18 °C, with a reverse blue-shift of the LSP wavelength (see Figure SI7b). A small hysteresis is observed during the heating−cooling cycles of pNIPAM, which can be attributed to the formation of inter- and intrachain hydrogen bonding between C═O and H−N groups above the LCST, acting as cross-linking points modifying the swelling cycle (see Figure SI7c).[46]

In order to quantify and compare the ability of the different GNR arrays to report the thermosensitive polymer state,

through a change in refractive index, we introduced the ratio γ = $\Delta\lambda_{LSP}/(fwhm_{LSP} \times \Delta T)$, where $fwhm_{LSP}$ represents the full width at half-maximum of the LSP band below the LCST, and ΔT represents the variation of temperature in the transition region (between 28 and 40 °C). In this region, the sigmoid curve can be approximated as a straight line. As shown in Figure SI.9, the ratio γ is increasing with the aspect ratio of the GNRs (for samples A and B). For instance, we found $\gamma \approx 10^{-2}$ for the GNR array with an aspect ratio of r = 2.4, and $\gamma \approx 6 \times 10^{-3}$ for the GNR array with an aspect ratio of r = 1.3 (sample A). We can conclude that for the optical reading of the phase transition the use of GNRs with r = 2.4 leads to a ∼2 times more sensitive system than that for the GNRs with r = 1.3.

The influence of the shell thickness was investigated for the optical reading of the phase transition. The temperature dependence of the LSP shift for samples A and B is presented in Figure 7 for a fixed GNR aspect ratio of r = 2.3. As expected,
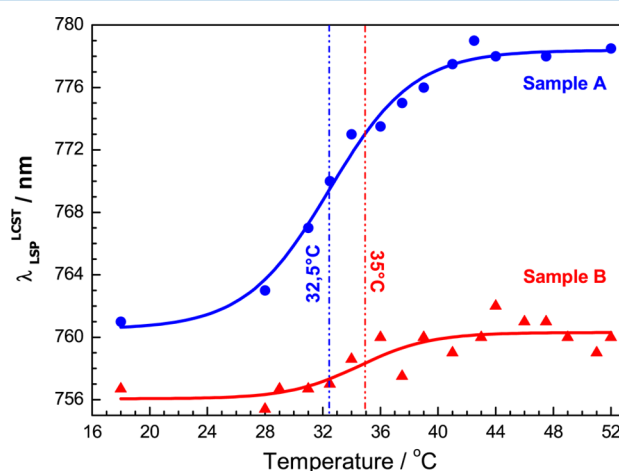
Figure 7. Plot of the temperature dependence of the longitudinal LSP wavelength for a GNR array with an aspect ratio of r = 2.3, with two different pNIPAM thicknesses (corresponding to samples A and B). For sample A, the blue circles represent the experimental data, and the blue solid line, the sigmoid curve fitting the experimental data. For sample B, the red triangles represent the experimental data, and the red solid line, the sigmoid curve fitting the experimental data. The maximum values deduced from the derivatives of the sigmoid curves are represented by dashed vertical lines (in blue for sample A and in red for sample B).

the slope of the sigmoid curve fitted from the experimental data is lower when the shell is thinner. From the derivative of the curves, we could deduce a maximum at ∼32.5 °C from sample A. However, in the case of the thinner shell (sample B), we found a maximum close to 35 °C, which is far from the expected value of the LCST given in literature. This discrepancy is attributed to the fact that the fitting of the experimental data is not satisfying because of the very weak LSP shift $\Delta\lambda_{LSP}^{LCST}$ measured (∼3 nm). As a consequence of the weak LSP shift, the aspect ratio γ is lower for the GNRs of sample B, whatever the aspect ratio, compared to the GNRs of sample A (Figure SI.9).

■ CONCLUSION

In summary, lithographic core−shell GNR@pNIPAM systems were elaborated as efficient models in order to investigate properly the influence of the nanoparticle anisotropy and the organic layer thickness on sensitivity to the local environment.

Table 3. Number of Dipoles Considered for the Core−Shell Targets of Various Dielectric Thicknesses H_{OVL}, with the Corresponding Calculated LSP Wavelengths

H_{OVL} (nm)	0	6	14	20	26	30	40	∞
N_d	37 200	60 388	103 818	146 970	199 818	372 200	367 900	37 200
λ_{LSP} (nm)	674	682	687	690	692	694	696	698

The optimization of the GNRs' aspect ratio as well as the shell thickness in order to provide a maximum of LSP shift when varying the external temperature was obtained for GNR aspect ratios in the range of $r \approx 2.4$−2.6 and a pNIPAM thickness $h_{pNIPAM} = 25$ nm (in the dry state). The thermosensitive behavior of the GNR@pNIPAM structures versus the temperature has been also evidenced by AFM measurements in a liquid cell: it was possible to estimate a thickness on the order of 50% of the height of the pNIPAM in the swollen regime, in the region of the phase transition. A factor of sensitivity has been introduced in order to quantify and compare the ability of such samples to report the thermosensitive polymer states: it was found that for the optical reading of the phase transition the use of GNRs with $r = 2.4$−2.6 leads to a 3 times more sensitive plasmonic system than for GNRs with $r = 1.3$. These results highlight the importance of a proper description and characterization of hybrid systems in order to provide designed criteria for efficient stimuli-responsive devices in the context of a new generation of thermoswitchable platforms for sensing and active plasmonic applications.[47,48] In the context of nanothermometry, such hybrid devices may be used as a direct temperature-sensing system in order to estimate the temperature increase of the plasmonic structures under LSP excitation. In the context of biomedical applications, pNIPAM microgels are also investigated for targeted drug delivery or tissue engineering.[49]

EXPERIMENTAL SECTION

Organic Materials. Reagent-grade solvents were purchased from VWR, Sigma-Aldrich, and Alfa Aesar. 2-Bromoisobutyryl bromide (97%, Alfa Aesar), triethylamine (TEA) (99%, Merck), Cu(I)Br (98%, Sigma-Aldrich), N,N,N',N'',N''-pentamethyldiethyltriamine (PMDETA) (99%, Acros Organics), *tert*-butyl nitrite (90%, Sigma-Aldrich), and 2-(4-aminophenyl)-ethanol (98%, Sigma-Aldrich) were used as received. *N*-Isopropylacrylamide (NIPAM) (99%, Sigma-Aldrich) was purified by recrystallization in *n*-hexane solution.

Synthesis of 4-Hydroxyethylbenzene Diazonium Tetrafluoroborate Salt ($+N_2$-C_6H_4-CH_2-CH_2-OH). A stirred solution of 2-(4-aminophenyl)ethanol (0.69 g) and HBF_4 (1.8 mL) in acetonitrile (3 mL) at −10 °C was added dropwise to a solution of *tert*-butylnitrite (0.63 g) in acetonitrile (3 mL) at −10 °C. The resulting mixture was kept overnight at −10 °C. The precipitate was washed three times with 50 mL of diethyl ether, then with 50 mL of acetone, and finally evaporated under vacuum. The 4-(2-hydroxyethyl)benzene diazonium tetrafluoroborate salt was stored at −10 °C.

Grafting of the Polymer. *Initiator-Modified Gold Surface.* The atom transfer radical polymerization initiator was grafted in two steps. (i) Spontaneous grafting of 4-hydroxyethylbenzene diazonium tetrafluoroborate salt (noted $HO(CH_2)_2BD$) was achieved on a cleaned gold nanostructure-coated ITO (indium−tin oxide) wafer by incubation at room temperature for 4 h with a concentration of 10^{-2} M for sample A and 5×10^{-3} M for sample B. (ii) Then, the terminal hydroxyl groups were treated with 2-bromoisobutyryl bromide

(0.1 M, toluene) in the presence of TEA (0.12 M) for 5 min to produce bromo-terminated ester groups. The Br-terminated gold surfaces are abbreviated as Au−Br.

Atomic Transfer Radical Polymerization (ATRP) of NIPAM. Solutions were prepared and kept at room temperature during degassing by passing a continuous stream of argon through the solution while being stirred. The polymerization solution was prepared by adding a solution of an organometallic catalyst to a solution of NIPAM monomer. The extremely oxygen sensitive organometallic catalyst was prepared by adding a 5 mL solution of PMDETA in MeOH (200 μL, 1 mmol) to 30 mg of CuBr (0.2 mmol). A 3 mL portion of the resulting green solution (which could possibly turn blue due to the presence of $CuBr_2$ and provide unsuccessful ATRP) was added to a solution of NIPAM monomer (2 g, 18 mmol) in 9 mL of deionized water under a continuous stream of argon. The polymerization solution was allowed to stir while degassing for 15 min and then transferred into a degassed flask containing the initiator-modified gold surface (Au−Br). The resulting solution was allowed to stir at room temperature under argon for various times (60 min for sample A and 30 min for sample B). Substrates were then removed from the flask, rinsed thoroughly with water and ethanol, and subsequently dried under a flush of argon.

DDA Calculations. The DDA method was employed to model the LSPR wavelength of the core−shell GNRs. This method is one particular discretization method for solving Maxwell's equations in the presence of a particle in which the continuum particle is replaced by an array of polarizable *N*-point dipoles located on cubic lattice sites. Computations were performed using the DDSCAT 7.0 software, which calculates efficiency factors, $Q_{ext} = C_{ext}/\pi a_{eff}^2$ (C_{ext} is the extinction cross section and a the effective radius of the particle).[37,38] In the calculation, we consider that the gold nanorod can be represented by a rectangle ended by two hemispherical edges with a main axis of 112 nm, a short axis of 60 nm, and height of 50 nm. A dielectric overlayer ($n = 1.4$) of different thicknesses covers the gold part, and the whole target is immersed in water ($n_{H_2O} = 1.33$). The number of dipoles (N_d) depends on the overlayer thickness (H_{OVL}) (see Table 3): from 37 200 for $H_{OVL} = 0$ nm to 367 900 for $H_{OVL} = 40$ nm. The distance between each dipole remains constant, 2 nm. The interaction between the GNRs is taken into account (interparticle distance $\Lambda = 280$ nm), but not with the substrate, enabling us to make only qualitative comparisons between the experimental and calculated spectra.

Instrumentation. AFM measurements are performed in tapping mode with a contact mode cantilever (on a SPM Nanoscope III, Veeco, Bruker) atomic force microscope. Contact mode AFM is applied in water with a contact SNL-10 silicon tip commercially available from Bruker. Vibration frequency of the tip is chosen at around 7 Hz to achieve a stable signal to noise ratio in water. AFM images were processed and analyzed using the application WSxM and FabViewer [WxSM, FabViewer].

ASSOCIATED CONTENT

S Supporting Information

The Supporting Information is available free of charge on the ACS Publications website at DOI: 10.1021/acsphotonics.5b00280.

> Additional details about the geometrical parameters of the bare GNRs (Table 1) and additional figures (Figure SI1 to Figure SI9) illustrating the content of the paper, including XPS and AFM measurements, extinction spectra of the GNR arrays before and after the pNIPAM grafting, and temperature dependence of the longitudinal LSP wavelength of the GNR@pNIPAM structures (PDF)

AUTHOR INFORMATION

Corresponding Authors
*E-mail: mangeney@univ-paris-diderot.fr.
*E-mail: nordin.felidj@univ-paris-diderot.fr.

Notes
The authors declare no competing financial interest.

REFERENCES

(1) Sun, Y.; Jiang, L.; Zhong, L.; Jiang, Y.; Chen, X. Towards Active Plasmonic Response Devices. *Nano Res.* **2015**, *8*, 406−417.

(2) Berthelot, J.; Bouhelier, A.; Huang, C.; Margueritat, J.; Colas Des Francs, G.; Finot, E.; Weeber, J.-C.; Dereux, A.; Kostcheev, S.; El-Ahrach, H. I.; Baudrion, A. L.; Plain, J.; Bachelot, R.; Royer, P.; Wiederrecht, G. Tuning of an Optical Dimer Nanoantenna by Electrically Controlling Its Load Impedance. *Nano Lett.* **2009**, *9*, 3914−3921.

(3) Liu, X.; Wang, X.; Zha, L.; Lin, D.; Yang, J.; Zhou, J.; Zhang, L. Temperature- and pH-Tunable Plasmonic Properties and SERS Efficiency of the Silver Nanoparticles Within the Dual Stimuli-Responsive Microgels. *J. Mater. Chem. C* **2014**, *2*, 7326−7335.

(4) König, T. A. F.; Ledin, P. A.; Kerszulis, J.; Mahmoud, M. A.; El-Sayed, M. A.; Reynolds, J. R.; Tsukruk, V. V. Electrically Tunable Plasmonic Behavior of Nano-Cube-Polymer Nanomaterials Induced by a Redox-Active Electrochromic Polymer. *ACS Nano* **2014**, *8*, 6182−6192.

(5) Baudrion, A.-L.; Perron, A.; Veltri, A.; Bouhelier, A.; Adam, P.-M.; Bachelot, R. Reversible Strong Coupling in Silver Nanoparticle Arrays Using Photochromic Molecules. *Nano Lett.* **2013**, *13*, 282−286.

(6) Coursault, D.; Grand, J.; Zappone, B.; Ayeb, H.; Lévi, G.; Félidj, N.; Lacaze, E. Linear Self-Assembly of Gold Nanoparticles Within Liquid Crystal Defect Arrays. *Adv. Mater.* **2012**, *24*, 1461−1465.

(7) Zhou, X.; Deeb, C.; Kostcheev, S.; Wiederrecht, G.; Adam, P.-M.; Béal, J.; Plain, J.; Gosztola, D.; Grand, J.; Félidj, N.; Wang, H.; Vial, A.; Bachelot, R. Selective Functionalization of the Nanogap of a Plasmonic Dimer. *ACS Photonics* **2015**, *2*, 121−129.

(8) Kreibig, U.; Vollmer, M. In *Optical Properties of Metal Clusters*; Springer: New York, 1995.

(9) Maier, S. A. In *Plasmonics: Fundamentals and Applications*; Springer Science: New York, 2007.

(10) Félidj, N.; Truong, S. L.; Aubard, J.; Lévi, G.; Krenn, J. R.; Hohenau, A.; Leitner, A.; Aussenegg, F. R. Gold Particle Interaction in Regular Arrays Probed by Surface Enhanced Raman Scattering. *J. Chem. Phys.* **2004**, *120*, 7141−7146.

(11) Leroux, Y.; Lacroix, J. C.; Fave, C.; Stockhausen, V.; Felidj, N.; Grand, J.; Hohenau, A.; Krenn, J. R. Active Plasmonic Devices with Anisotropic Optical Response: A Step Toward Active Polarizer. *Nano Lett.* **2009**, *9*, 2144−2148.

(12) Brown, A. M.; Sheldon, M. T.; Atwater, H. A. Electrochemical Tuning of the Dielectric Function of Au Nanoparticles. *ACS Photonics* **2015**, *2*, 459−464.

(13) Schaming, D.; Nguyen, V.-Q.; Martin, P.; Lacroix, J.-C. Tunable Plasmon Resonance of Gold Nanparticles Functionalized by Electro-active Bisthienylbenzene Oligomers or Polythiophene. *J. Phys. Chem. C* **2014**, *118*, 25158−25166.

(14) Contreras-Caceres, R.; Pastoriza-Santos, I.; Alvarez-Puebla, R. A.; Perez-Juste, J.; Fernandez-Barbero, A.; Liz-Marzan, L. M. Growing Au/Ag Nanoparticles within Microgel Colloids for Improved Surface-Enhanced Raman Scattering Detection. *Chem. - Eur. J.* **2010**, *16*, 9462−9467.

(15) Alvarez-Puebla, R. A.; Contreras-Caceres, R.; Pastoriza-Santos, I.; Perez-Juste, J.; Liz-Marzan, L. M. Au@pNIPAM Colloids as Molecular Traps for Surface Enhanced, Spectroscopic, Ultra-Sensitive Analysis. *Angew. Chem., Int. Ed.* **2009**, *48*, 138−143.

(16) Barhoumi, A.; Wang, W.; Zurakowski, D.; Langer, R. S.; Kohane, D. S. Photothermally Targeted Thermosensitive Polymer-Masked Nanoparticles. *Nano Lett.* **2014**, *14*, 3697−3701.

(17) Gehan, H.; Mangeney, C.; Aubard, J.; Levi, G.; Hohenau, A.; Krenn, J. R.; Lacaze, E.; Felidj, N. Design and Optical Properties of Active Polymer-Coated PlasmonicNanostructures. *J. Phys. Chem. Lett.* **2011**, *2*, 926−931.

(18) Gotschy, W.; Vonmetz, K.; Leitner, A.; Aussenegg, F. R. Thin Films by Regular Patterns of Metal Nanoparticles: Tailoring the Optical Properties by Nanodesign. *Appl. Phys. B: Lasers Opt.* **1996**, *63*, 381−384.

(19) Schild, H. G. Poly(N-isopropylacrylamide): Experiment, Theory and Application. *Prog. Polym. Sci.* **1992**, *17*, 163−249.

(20) Malham, I.; Bureau, L. Density Effects on Collapse, Compression, and AdhesIOn of Thermorepsonsive Polymer Brushes. *Langmuir* **2010**, *26*, 4762−4768.

(21) Toma, M.; Jonas, U.; Mateescu, A.; Knoll, W.; Dostalek, J. Active Control of SPR by Thermoresponsive Hydrogels for Biosensor Applications. *J. Phys. Chem. C* **2013**, *117*, 11705−11712.

(22) Inoue, H.; Kuwahara, S.; Katayama, K. The Whole Process of Phase Transition and Relaxationof Poly(N-isopropylacrylamide) Aqueous Solution. *Phys. Chem. Chem. Phys.* **2013**, *15*, 3814−3820.

(23) Karg, M.; Pastoriza-Santos, I.; Perez-Juste, J.; Hellweg, T.; Liz-Marzan, L. M. Nanorod-coated PNIPAM Microgels: Thermoresponsive Optical Properties. *Small* **2007**, *3*, 1222−1229.

(24) Rodriguez-Fernandez, J.; Fedoruk, M.; Hrelescu, C.; Lutich, A. A.; Feldmann, J. Triggering the Volume Phase Transition of Core-Shell Au Nanorod-Microgel Nanocomposites with Light. *Nanotechnology* **2011**, *22*, 245708.

(25) Li, B.; Smilgies, D. M.; Price, A. D.; Huber, D. L.; Clem, P. G.; Fan, H. Poly(N-isopropylacrylamide) Surfactant-Functionalized Responsive Silver Nanoparticles and Superlattices. *ACS Nano* **2014**, *8*, 4799−4804.

(26) Contreras-Cácares, R.; Pacifico, J.; Pastoriza-Santos, I.; Perez-Juste, J.; Fernandez-Barbero, A.; Liz-Marzan, L. Au@pNIPAM Thermosensitive Nanostructures: Control over Shell Cross-linking, Overall Dimensions, and Core Growth. *Adv. Funct. Mater.* **2009**, *19*, 3070−3076.

(27) Muller, M. B.; Kuttner, C.; Konig, T. A. F.; Tsukruk, V. V.; Forster, S.; Karg, M.; Fery, A. Plasmonic Library Based on Substrate Supported Gradiential Plasmonic Arrays. *ACS Nano* **2014**, *8*, 9410−9421.

(28) Tagliazucchi, M.; Blaber, M. G.; Schatz, G. C.; Weiss, E. A.; Szleifer, I. Optical Properties of Responsive Hybrid Au@Polymer Nanoparticles. *ACS Nano* **2012**, *6*, 8397−8406.

(29) Becker, J.; Trugler, A.; Jakab, A.; Hohenester, U.; Sonnichsen, C. The Optimal Aspect Ratio of Gold Nanorods for Plasmonic Bio-sensing. *Plasmonics* **2010**, *5*, 161−167.

(30) Gehan, H.; Fillaud, L.; Chehimi, M.; Aubard, J.; Hohenau, A.; Felidj, N.; Mangeney, C. Thermo-induced Electromagnetic Coupling in Gold/Polymer Hybrid Plasmonic Structures Probed by Surface-Enhanced Raman Scattering. *ACS Nano* **2010**, *4*, 6491−6500.

(31) Pinson, J.; Podvorica, F. Attachment of Organic Layers to Conductive or Semiconductive Surfaces by Reduction of Diazonium Salts. *Chem. Soc. Rev.* **2005**, *34*, 429−439.

(32) Mahouche-Chergui, S.; Gam-Derouich, S.; Mangeney, C.; Chehimi, M. M. Aryl Diazonium Salts: a New Class of Coupling Agents for Bonding Polymers, Biomacromolecules and Nanoparticles to Surfaces. *Chem. Soc. Rev.* **2011**, *40*, 4143−4166.

(33) Hohenau, A.; Ditlbacher, H.; Lamprecht, B.; Krenn, J. R.; Leitner, A.; Aussenegg, F. R. Electron Beam Lithography, a Helpful Tool for Nanooptics. *Microelectron. Eng.* **2006**, *83*, 1464−1467.

(34) Matyjaszewski, K. Atom Transfer Radical Polymerization (ATRP): Current Status and Future Perspectives. *Macromolecules* **2012**, *45*, 4015−4039.

(35) Jiao, A.; Trosper, N. E.; Yang, H. S.; Kim, J.; Tsui, J. H.; Frankel, S. D.; Murry, C. E. Thermoresponsive Nanofabricated Substratum for the Engineering of Three-Dimensional Tissues with Layer-by-Layer Architectural Control. *ACS Nano* **2014**, *8*, 4430−4439.

(36) Li, Q.; Zhang, W.; Zhao, D.; Qiu, M. Photothermal Enhancement in Core-Shell Structured Plasmonic Nanoparticles. *Plasmonics* **2014**, *9*, 623−630.

(37) Purcell, E. M.; Pennypacker, C. R. Scattering and Absorption of Light by Nonspherical Dielectric Grains. *Astrophys. J.* **1973**, *186*, 705−714.

(38) Draine, B. T.; Flatau, P. J. *User Guide for the Discrete Dipole Approximation Code DDSCAT7.0*, http://arxiv.org.abs.0809.0337.

(39) Horcas, I; Fernandez, R.; Gémez-Rodéguez, J. M.; Colchero, J.; Gémez-Herrero, J.; Baro, A. M. A Software for Scanning Probe Microscopy and a Tool for Nanotechnology. *Rev. Sci. Instrum.* **2007**, *78*, 013705.

(40) Malham, I. B.; Bureau, L. Density Effects on Collapse, Compression, and Adhesion of Thermoresponsive Polymer Brushes. *Langmuir* **2010**, *26*, 4762−4768.

(41) Alexander, S. Adsorption of Chain Molecules with a Polar Head a Scaling Description. *J. Phys. (Paris)* **1977**, *38*, 983−987.

(42) de Gennes, P. G. Conformations of Polymers Attached to an Interface. *Macromolecules* **1980**, *13*, 1069−1075.

(43) Ishida, N.; Biggs, S. Direct Observation of the Phase Transition for a Poly(N-isopropylacryamide) Layer Grafted onto a Solid Surface by AFM and QCM-D. *Langmuir* **2007**, *23*, 11083−11088.

(44) Gabudean, A. M.; Focsan, M.; Astilean, S. Gold Nanorods Performing as Dual-Modal Nanoprobes via Metal-Enhanced Fluorescence (MEF) and Surface-Enhanced Raman Scattering (SERS). *J. Phys. Chem. C* **2012**, *116*, 12240−12249.

(45) Baffou, G.; Quidant, R. Nanoplasmonics for Chemistry. *Chem. Soc. Rev.* **2014**, *43*, 3898−3907.

(46) Deshmukh, S.; Kamath, G.; Suthar, K. J.; Mancini, D. C.; Sankaranarayanan, S. K. Non-Equilibrium Effects Evidenced by Vibrational Spectra during the Coil-to-Globule Transition in Poly-(N-isopropylacrylamide) Subjected to an Ultrafast Heating-Cooling Cycle. *Soft Matter* **2014**, *10*, 1462−1480.

(47) Jaque, D.; Vetrone, F. Luminescence Nanothermometry. *Nanoscale* **2012**, *4*, 4301−4326.

(48) Brites, C.; Lima, P.; Silva, N.; Millan, A.; Amaral, V.; Palacio, F. Thermometry at the Nanoscale. *Nanoscale* **2012**, *4*, 4799−4829.

(49) Guan, Y.; Zhang, Y. PNIPAM Microgels for Biomedical Applications: From Dispersed Particles to 3D Assemblies. *Soft Matter* **2011**, *7*, 6375−6384.